REVEALING MULTIPLE GLOBAL TECTONIC PATTERNS ON MERCURY. Christian Klimczak[1], Kelsey T. Crane[2], and Paul K. Byrne[3], [1]Department of Geology, University of Georgia, Athens, GA 30602, USA (klimczak@uga.edu); [2]Department of Geosciences, Mississippi State University, Mississippi State, MS 39762, USA; [3]Department of Earth and Planetary Sciences, Washington University in St. Louis, St. Louis, MO 63130, USA.

Introduction: The innermost planet abounds with tectonic landforms. Multiple mapping efforts of such landforms on global, regional, and local scales have resulted in a series of tectonic maps [e.g., 1–5]. Tectonic landforms on Mercury can generally be classified into one of two groups: either those associated with thrust faulting and thus crustal shortening; or those that include joints and normal faults, and so represent extensional strains. Proper mapping and analysis of these landforms, such as assessments of strain amounts or structure orientations, yields valuable information on the tectonic processes that operated when these structures formed and developed. Although previous such assessments have focussed heavily on global-scale amounts of shortening strains [e.g., 1,5], the systematic study of the orientations of structures and the matching of predictions of global tectonic processes to structural observations have received less attention. Here, we compiled several map datasets into one internally consistent global map, extracted all structure orientations, and searched for global patterns to gain insight into what global tectonic processes have operated on Mercury.

Methods: We compiled a global tectonic map of Mercury (Fig. 1) from the global thrust fault map by [1], a map of thrust faults in Borealis Planitia [2], maps of intra-basin structures [3], and extensional structures in ghost craters [4].

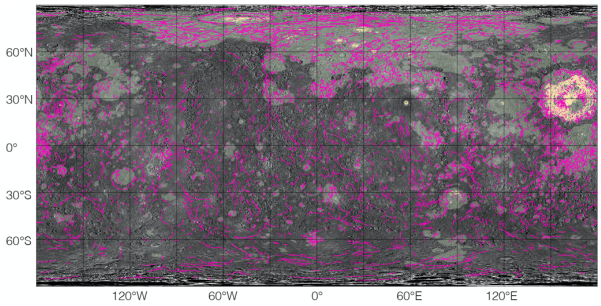

Fig. 1) Global tectonic map, compiled from [1–4], shown in equirectangular projection. Magenta and salmon lines symbolize shortening and extensional structures, respectively. The base map is the MESSENGER monochrome mosaic [6], and lightly shaded areas are smooth plains [7].

Next, we standardized these different map products by removing all vertices that did not contribute toward the shape of the map traces. We then split the map segments at the remaining vertices and computed all segment lengths and azimuths, treating those azimuths as the strikes of the faults underlying the landforms. We then divided Mercury into multiple geographic regions and extracted and grouped the length and azimuths of all segments of each region. To best visualize structure orientations, we calculated the optimal bin size for which a rose diagram—a display of a circular distribution of directional data—would best illustrate patterns for length-weighted azimuths. We then color-coded each rose diagram by the structure density for its geographic region (Fig. 2-4).

Global tectonic patterns: The global tectonic map highlights the locations of shortening (magenta lines) and extensional (salmon lines) structures across Mercury (Fig. 1). Thrust faults are globally distributed, whereas normal faults are almost wholly found in smooth plains units contained within impact structures [3]. We investigated all structure orientations with respect to four phenomena: global contraction, tidal despinning, the formation of the Caloris basin, and effects resulting from Mercury's spin-orbit resonance with the sun.

Global contraction. The sustained cooling and associated shrinking of Mercury is responsible for the widespread formation of thrust faults across Mercury. Operating by itself, global contraction is predicted to yield a pattern of randomly oriented thrust faults [8]. However, our analysis shows preferred orientations of faults in nearly all regions of Mercury (Fig. 2). Although global contraction is clearly the principal reason for the formation and growth of thrust faults, the orientations of these structures must have been influenced by one or more overlapping tectonic processes.

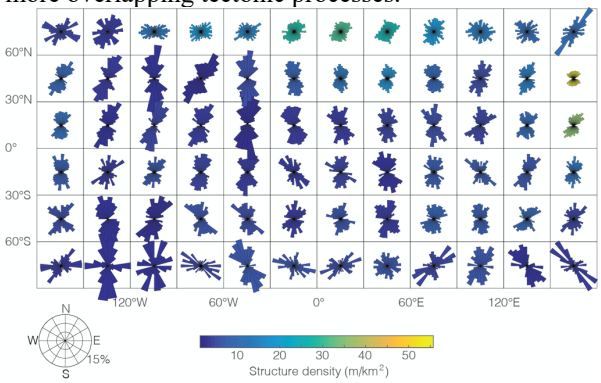

Fig. 2) Latitudinal and longitudinal variations in structure orientations represented by one rose diagram per 30° × 30° geographical bin.

Tidal spindown. Tidal despinning overlapping global contraction is one scenario that predicts

latitudinal patterns, with N–S-oriented thrusts in equatorial/mid-latitudinal regions and no preferred orientations at the poles [9]. We do indeed observe Mercury's tectonic structures to be preferentially oriented N–S in the equatorial/mid-latitudinal regions, but they show other strongly preferred orientations in many geographic regions, especially near the poles (Fig. 2). This finding indicates that additional processes have influenced Mercury's structure orientations.

The Caloris-forming impact. The giant Caloris-forming impact may have produced basin-radial and circumferential fractures that could have been reactivated as thrust faults by global contraction. We divided Mercury into regions bounded by markers that are radial and concentric to Caloris, extracted the data, and replotted new rose diagrams accordingly (Fig. 3). Results show that the latitudinal N–S pattern obvious in Fig. 2 is less apparent and that at least half of the bins have structures that display a dominance of basin-radial and/or concentric faults, even far from the basin. This finding emphasizes that re-binning spatial tectonic data into different geographic regions is essential for interpretations of processes that are not expected to result in latitudinal patterns. Furthermore, the Caloris-forming impact likely introduced an expansive fracture network that was then reactivated, at least in places, as thrust faults by global contraction.

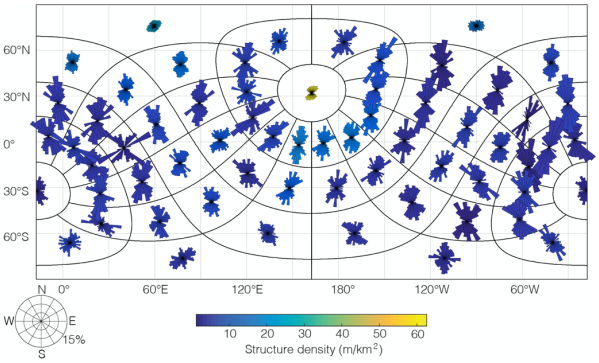

Fig. 3) Rose diagrams depicting variations in structure orientations around the Caloris basin. Geographic bins are defined by basin-radial markers in 30° intervals, and by basin-concentric markers in increments of Caloris basin diameter. Map projection is centered to the Caloris basin.

Orbital effects on tectonics. Mercury is locked in a 3:2 spin–orbit resonance with the Sun, with the orbit showing a marked eccentricity of ~0.2. This configuration results in an asymmetric temperature distribution across Mercury's surface, causing two equatorial hot poles at 0° and 180° longitudes, and leading to considerable tides. Surface temperature variations affect the lithosphere, causing variations in its strength and thickness that follow the hot pole geometries [10]. Mercury's tides may not be pronounced enough to directly produce rock failure, but tidal stresses superposed on global contraction, paired with the fatiguing resulting from tides acting over billions of years, may also influence the patterns and strength within the lithosphere.

To test this hypothesis, we divided Mercury into regions bounded by markers radial and concentric to the hot poles, extracted the fault map data, and plotted the new rose diagrams accordingly (Fig. 4). We find that, again, the N–S pattern is less pronounced with this geographic binning, but that instead structure orientations follow radial and concentric patterns around the hot poles in many locations (Fig. 4). Such patterns imply that insulation-driven strength variations and/or tidal stresses superposed on global contraction have influenced strain patterns on Mercury.

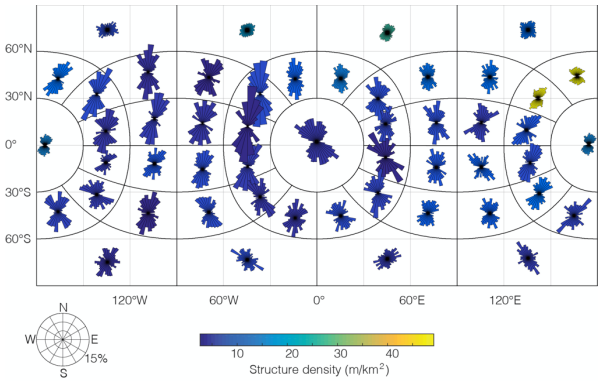

Fig. 4) Variations of fault orientations around Mercury's hot poles at (0°N, 0°E) and (0°N, 180°E). Geographic bins are defined by 30° radial and concentric markers centered on each hot pole.

Conclusion: Analyses of fault orientations using geographic binning specifically tied to the geometries of global tectonic phenomena reveal patters that otherwise go unrecognized. Our results for the binning configurations we describe here (Figs. 2-4) show that multiple processes likely overlapped to produce Mercury's global tectonic pattern. Further work may show if other tectonic phenomena, such as patterns tied to regional tectonics, add to the variation of fault orientation.

References: [1] Byrne P. K. et al. (2014) *Nat. Geosci., 7,* 301–307. [2] Crane K. T. & Klimczak C. (2019) *Icarus, 317,* 66–80. [3] Byrne P. K. et al. (2018) In *Mercury: The View after MESSENGER (Eds. Solomon S. C. et al.),* 249–286. [4] Klimczak C. et al. (2012) *JGR Planets, 117,* E00L03. [5] Watters T. R. et al. (2021) *GRL, 48,* e2021GL093528. [6] Denevi B. W. et al. (2018) *Space. Sci. Rev., 214:2,* 52pp. [7] Denevi B. W. et al. (2013) *JGR Planets, 118,* 891–907. [8] Melosh H. J. & McKinnon W. B. (1989) In *Mercury (Eds. Vilas F. et al.),* 374–400. [9] Klimczak C. et al. (2015) *EPSL, 416,* 82–90. [10] Williams J.-P. et al. (2011) *JGR Planets, 116,* E101008.